Subsidence associated with oil extraction, measured from time-series analysis of Sentinel-1 data : case study of the Patos-Marinza oil field, Albania

Marianne Métois[1], Mouna Benjelloun[1], Cécile Lasserre[1], Raphael Grandin[2], Laurie Barrier[2], Edmond Dushi[3], and Rexhep Koçi[3]

[1]Laboratoire de géologie de Lyon, Université de Lyon, Université Lyon 1, ENS de Lyon, CNRS, UMR 5276 LGL-TPE, F-69622 Villeurbanne, France
[2]Université de Paris, Institut de Physique du Globe de Paris, UMR 7154, F-75238 Paris cedex 05, France
[3]Institute of Geosciences, Polytechnic University of Tirana, Tirana, Albania

Correspondence: Marianne Métois (marianne.metois@univ-lyon1.fr)

Abstract. The Patos-Marinza oil field in Central Albania (40.71°N,19.61°E), operated since 1939, is one of the largest onshore fields in Europe. More than 7 millions oil barrels are extracted per year from the Messinian sandstone formations of the Durres Basin in the Albanian Peri-Adriatic Depression by the Bankers company operating the field since 2004.

In the region, the background seismicity culminated in December 2016, when a shallow seismic swarm developed in the oil
5   field, damaging houses and triggering the opening of a public inquiry. However, because of the lack of a dense local seismic array and incompleteness of historical catalogues for such moderate events, understanding whether this seismicity could be induced by the extraction/injection activities is an arduous task.

In this study, we take advantage of the new Sentinel-1 radar images acquired every 6 to 12 days over Albania to measure the surface displacement in the Myzeqeja plain and in the Patos-Marinza oil field in particular. Images from two ascending and
10   descending tracks covering the area are processed through a radar interferometry (InSAR) time-series analysis over the 2014 to 2018 time-span, providing consistent average Line-Of-Sight velocity maps and displacement time-series.

The regional deformation field exhibits a slow subsidence of the entire sedimentary basin relative to the highlands (at rates of 2.5 mm/yr), that we interpret as a combination of natural and man-induced compaction. This broad picture is complicated by a very strong local subsidence signal with rates as high as 15 mm/yr that spatially correlates with the Patos-Marinza oil field
15   and is maximal in the zone holding most of the operating horizontal wells, where Enhanced Oil Recovery techniques are used.

The striking spatial correlation between the maximum subsidence area and the active wells, as seen from optical images, argues in favor of an oil-extraction induced surface deformation. The observed surface deformation is well reproduced by elastic models mimicking the basin and reservoir compaction using planar crack dislocations. Such modeling provides a first-order estimation of the volumetric deflation rate in the oil reservoir (~0.2 Mm^3/yr). This strong subsidence signal, together
20   with the increase of the background seismicity since the oil field reactivation, are evidences of significant man-induced stress changes in the basin that should be further monitored and taken into account for seismic hazard assessment.

1 Introduction

Ground deformation due to oil or gas extraction from buried reservoirs has been reported for over a century. The first dramatic example of such a man-induced subsidence was observed in the Goose Creek oil field, Texas, from 1918 to 1925, with more

5 than 3 meters of vertical motion in the centre of the field (Pratt and Johnson, 1926; Coplin and Galloway, 1999). Since then, significant subsidence patterns have been observed over many productive oil or gas fields (e.g. Schoonbeek et al., 1976; van Thienen-Visser et al., 2015; Grebby et al., 2019), so much so that they are now usually monitored by the operating companies (Nagel, 2001). Indeed, since surface deformation is mostly due to reservoir depletion and compaction of the sedimentary layers, monitoring is a convenient indirect way to constrain the reservoir pressure and volume evolution through time. Soil and

10 surface instability caused by extraction can also substantially damage buildings and infrastructures (e.g. Doornhof et al., 2006). Furthermore, drilling processes and fluid extraction can change the pore pressure and stress field in the medium so much that anomalous seismic activity may be triggered (e.g. Segall, 1989; Segall et al., 1994; Ottemöller et al., 2005; Rubinstein and Mahani, 2015; Hettema et al., 2017).

In the last decades, the seek for ever increasing well productivity led to novel recovery methods based on horizontal drilling,

15 hydraulic fracturation, or deep injection of fluid or steam water to drive the oil out of the reservoir. The efficiency of these Enhanced Oil Recovery (EOR) techniques comes with bigger and faster changes in the deep stress field, increasing their potential for triggering local anomalous seismicity (Murray, 2013; Rubinstein and Mahani, 2015). For instance, the seismicity observed in the Oklahoma oil and gas field and its relationship with wastewater disposal has been extensively studied in the last years (Murray, 2013; Walsh and Zoback, 2015). The fact that extensive drilling and injection of fluids in the subsoil can trigger

20 moderate size earthquakes is thus now commonly admitted. The recent M_w 5.7, Pawnee earthquake, that ruptured a previously unmapped basement fault under the Oklahoma oil field, suggests that anthropogenic subsurface activities influence the stress state over a broad region (Grandin et al., 2017; Keranen et al., 2013), modifying substantially the regional seismic hazard (van Elk et al., 2017). However, monitoring the stress and pressure perturbations associated with an operated hydrocarbon field and understanding their relationship with the background seismicity require very dense seismic arrays, continuous monitoring of

25 deformation and a good knowledge of the reservoir characteristics (geometry, pressure history, etc).

Albania is a long-standing hydrocarbon productive country since natural bitumen surges were already exploited during Roman times (Verani and Ineichen, 1942). Effective oil drilling started at the beginning of the 20th century, taking advantage of the large deposits of gas and crude oil accumulated in the Ionian carbonates and siliclastic deposits of the Peri-Adriatic Depression in the Durres Basin in Albania (Fig. 1 and Sejdini et al., 1994). In the Patos-Marinza oil field (40.71°N,19.61°E)

30 operated since 1939, heavy crude oil contained in shallow Messinian siliclastic reservoirs has been extracted since 2004 by the Canadian firm Banker's petroleum (Figs. 2,3). To increase the productivity of this very large onshore oil field exploited using primary recovery techniques during the last century, EOR techniques including waterflooding, infill, thermal recovery and horizontal drilling have been applied to the northern part of the field, close to the Marinza village, starting in 2008 and
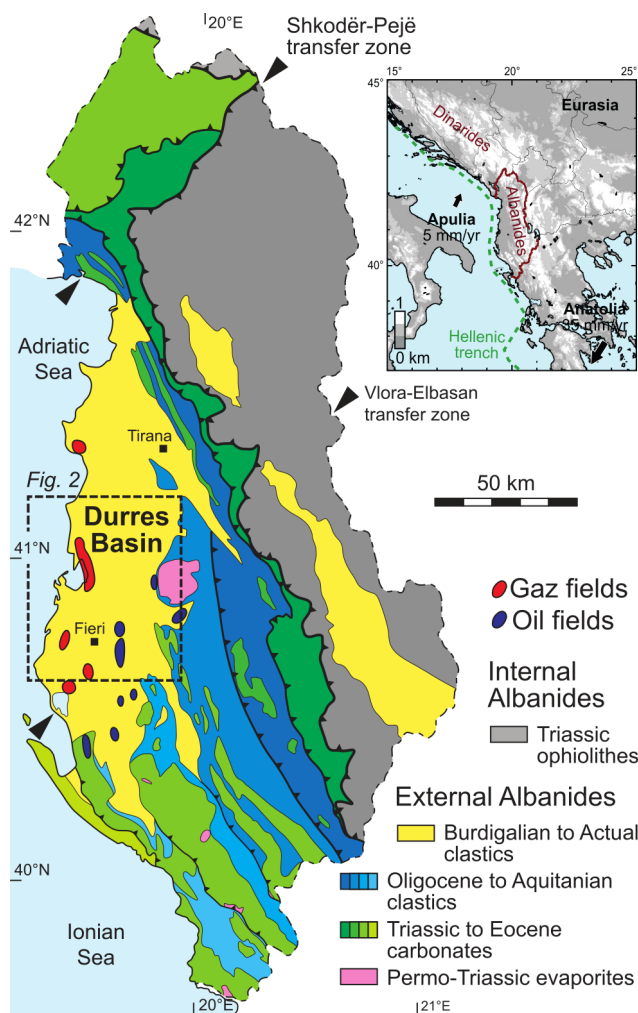
Figure 1. Simplified geological map of Albania. Oil and gas main fields are indicated in blue and red, respectively. Dashed rectangle is the study area as plotted in Fig. 2. Upper right inset shows the geographical location of Albania and regional kinematics with respect to stable Eurasia (Métois et al., 2015).

leading to spectacular productivity gains (BCP, 2015). Since then, several events have made the local population questioning about the risks associated with such an intensive extraction activity. In 2013, three $M_w \sim 4$ earthquakes that occurred in the area alarmed the population, yet claiming that the overall background seismicity had increased since at least 2012 (CAO complaint, filed 13 March 2013). On 1 April 2015, the Marinza village was evacuated due to leakages of natural gas during drilling

5   operations that contaminated water wells (Contamination report, 2015). More recently, in December 2016, a shallow seismic swarm (maximum M_L 4 at 2.9 km depth) developed, leading the government to open a public inquiry and enjoining Bankers to stop the water injection in the area (Report CAO, 2018).

Up to now, the lack of dense seismic network operating in the area over this period and the sparse knowledge of the pressure history of the reservoir prevent scientists to conclude on a potential causality between the oil extraction activity and the current seismicity (Report CAO, 2018). In this study, we take advantage of the dense spatio-temporal coverage of the new Sentinel-1 satellite radar images that cover the Patos-Marinza region with one image every 6 to 12 days to build consistent maps of the

5   surface displacement over the 2014 to 2018 time span using the Interferometric Synthetic-Aperture Radar (InSAR) technique. We then describe the subsidence and uplift patterns observed over the Patos-Marinza oil-field, quantify the associated motion rates, and suggest that such patterns are likely related to reservoir draining and associated compaction.

2   History, geological and seismotectonic setting of the Patos-Marinza oil field

In Albania, the oil and gas fields are concentrated in the external Albanides, composed of Mesozoic limestones that have been

10   thrusted, eroded and partially covered by Oligocene to Pliocene marine and deltaic deposits sedimentary series accumulating in the Peri-Adriatic Depression (Fig. 1 and Meço et al., 2000). The emerged part of this depression, i.e. the Durres Basin, hosts most of the productive fields in Albania, among which the Patos-Marinza field this study focuses on (Fig. 2). The shallowest formations encountered in this southern part of the Durres Basin are Holocene and Pleistocene lagoonal, marshy and alluvial deposits (Fig. 2-c) related to important variations in depositional environments of the Myzek plain and its shoreline (Ciavola,

15   1999). Today, the plain is drained by both the Skumbini and Semani rivers often flooding and changing their channel paths, and by a dense network of man-made canals built during the 1950–1980 period of reclaiming works for agriculture and public health purposes (Fig. 2-b, Shallari and Maughan, 2015). To the west, the basin is hardly above sea level and has deviated from its sedimentary equilibrium due to the recent anthropogenic reclamation. The coastline has thus drastically changed in the last decades (Ciavola and Simeoni, 1995; Shallari and Maughan, 2015), leading to a need for building artificial dikes. Apart from

20   agriculture, oil and gas extraction is the main economic income of the Fieri prefecture.

In the Durres Basin, the core of the Patos-Marinze oil field covers a ~45 km^2 zone over the Marinza and Zharrez municipalities in the Fieri prefecture. It is characterized by a very high spatial density of wells visible on satellite optical images (white areas in Fig. 2-a). In this Patos-Marinza oil field operated since 1939, a heavy crude oil that has migrated from Ionian Mesozoic source rocks is extracted from ~10°NW dipping Messinian sandstone reservoirs, located at depth ranging from few hundreds

25   of meters to roughly 2 km (Fig. 2-d, Silo et al., 2013; Prifti and Muska, 2013). Three units are currently exploited from top to bottom: the Gorani, Driza and Marinza series (Fig. 2-d), with various porosities (between 25 and 30%), compaction coefficients, and chemical and physical characteristics of the oil in place (Bennion et al., 2003). These series are therefore exploited using different extraction techniques (Fig. 3). The Albanian national oil company first operated the field using primary recovery methods until 1999, when secondary recovery techniques, in particular Cold Heavy Oil Production by Sand (CHOPS), started

30   to be used mainly in the Driza unit (Sejdini et al., 1994; Weatherill et al., 2005). Because of the high viscosity of the oil in place (30 to 3000 mPa.s following Weatherill et al., 2005), EOR methods have then been applied to the field by the Bankers company since 2009 in order to increase the production. While infill recovery is applied preferentially to the deepest Marinza unit, the Driza unit is now exploited using waterflooding, horizontal drilling and thermal recovery (Fig. 3 and BCP, 2015). As
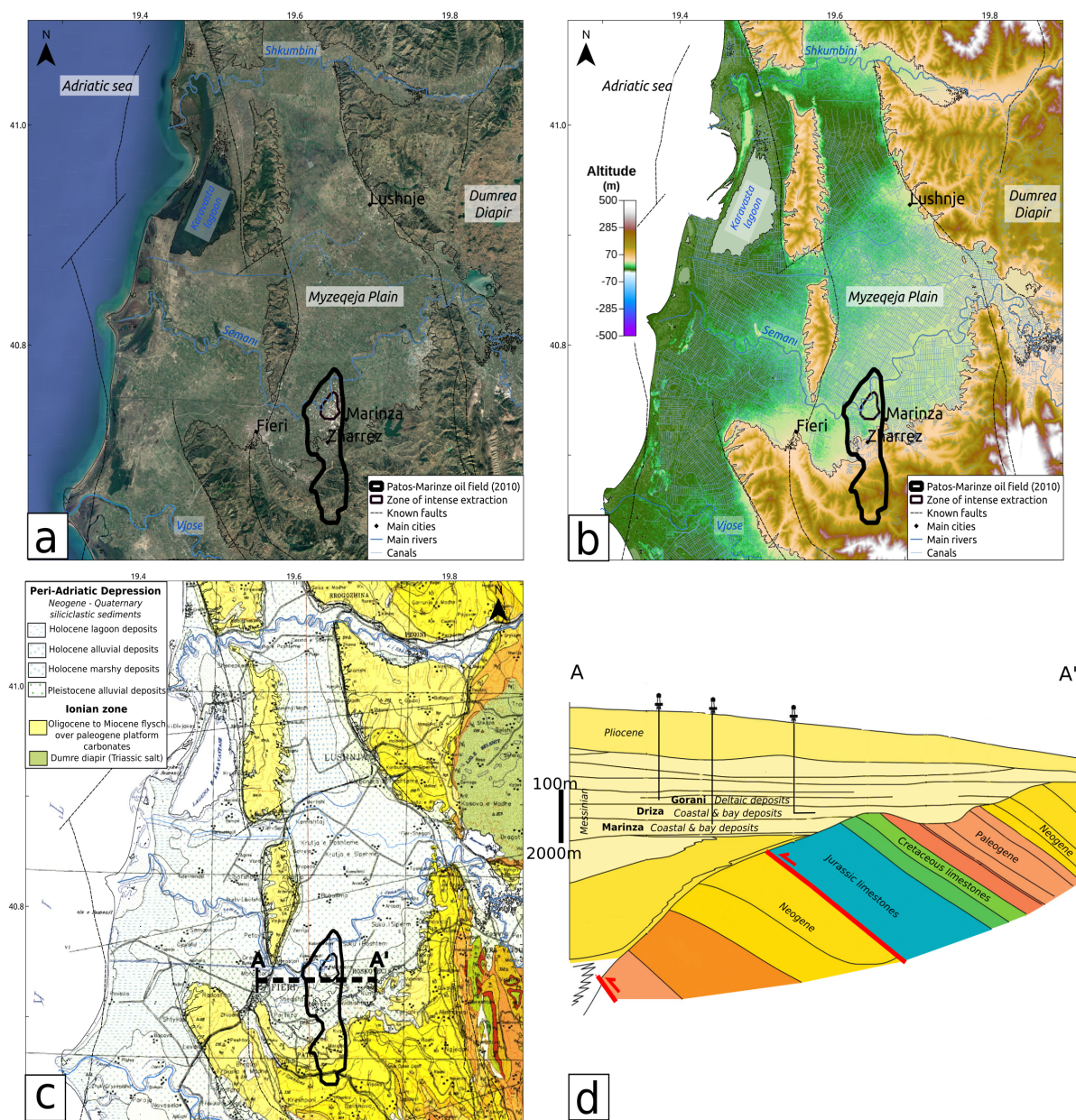
Figure 2. Anthropogenic, hydrological and geological context of the study area. The Patos-Marinza active oil-field (black bold line) is contoured based on BCP, 2015. It encompasses the zone where wells are the densest and extraction activity concentrates (thin black line). Faults (black dashed lines) are from Aliaj et al. (2000). a-Optical satellite image of the southern part of the Durres Basin in the Fieri prefecture (satellite images from the © Google Earth data base). b-Hydrology of the Myzeqeja plain. The network of man-made canals (in blue) is from TPGINC and is superimposed to the topography of the area (Farr and Kobrick, 2000). c-Extract of the Geological Map of Albania (simplified from Xhomo et al., 2002). The dotted bold line is the approximate position of the simplified geological transect presented in the panel d. d-West-East interpreted geological cross-section modified from Silo et al. (2013). The average depth of the Messinian sandstones oil-bearing formations drilled in the Patos-Marinza oil field is indicated together with the associated depositional environments. Faults in the underlying sedimentary series are plotted in red.
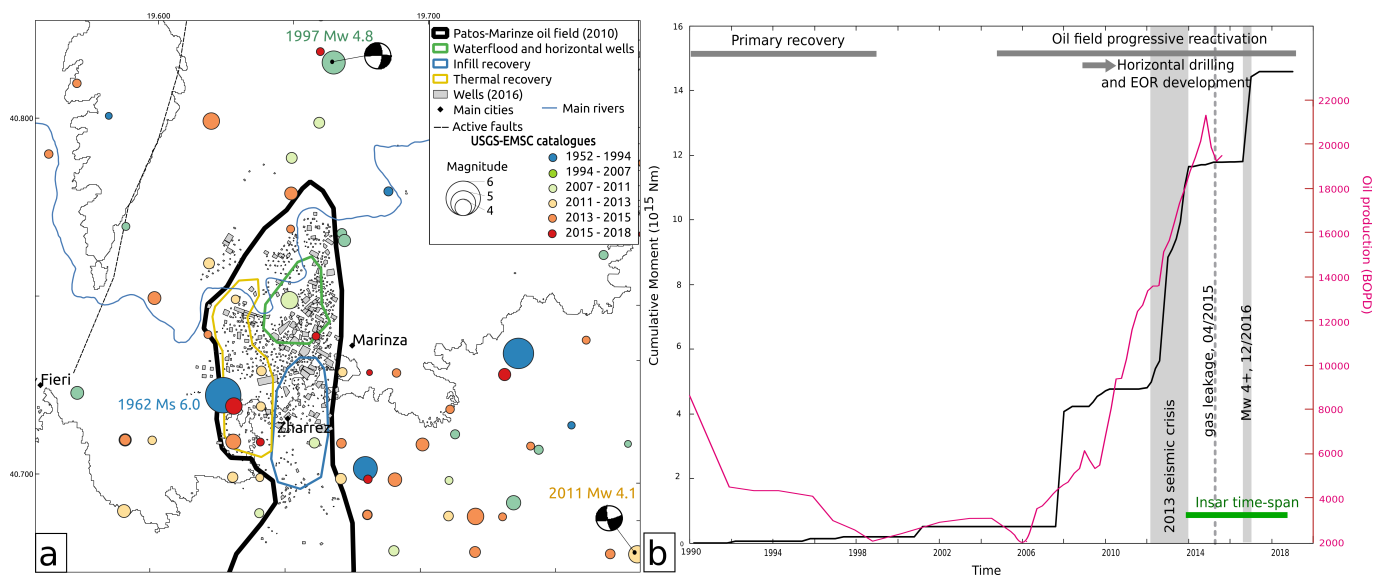
Figure 3. a- Exploitation extent and history of the Patos-Marinza oil field based on BCP, 2010. Major wells (grey rectangles of various sizes) have been mapped based on 2016 optical image (Fig. 2-a and satellite images from the Google Earth data base). Seismic events since 1950 are color-coded based on their occurrence time and sized depending on their magnitude (CSEM-EMSC; USGS, before and after 2004, respectively). b- Production evolution in Barrel Oil per Day (1 BOPD ~159 L) since 1990 (BCP, 2015) together with the cumulative released seismic moment based on USGS and EMSC catalogues for the region plotted in a-.

a result, more than 20,000 Barrel Oil Per Day (BOPD) were extracted from the oil field in 2014 (Fig. 3-B). The waterflooding area (green contour in Fig. 3-A) has also been the first zone to be reactivated in 2005 (BCP, 2015) and is the part of the field with the highest number of active wells, as mapped in Figure 3 using optical images from 2016. It is therefore reasonable to consider that this part of the field is currently the most intensely operated.

5   Because it is located between the Hellenic subduction zone and the Dinarides collision belts (Fig. 1), Albania is an earthquake-prone country that often experiences moderate earthquakes and has already suffered from M_w6+ devastating earthquakes (Jouanne et al., 2012; Métois et al., 2015). The external Albanides deform due to the ~5 mm/yr NE-moving Apulia microplate. They are characterized by thrust and strike-slip focal mechanisms attributed to active NNW-SSE thrust and fold structures and NE-SW trending transform zones (Aliaj et al., 2010; Jouanne et al., 2012). Large historical earthquakes are suspected to have

10 occurred in the past in the Fieri area based on narrations of the antique Apollonia destruction (II-III BC, 234 A.D Shebalin et al., 1998). A large M_S 6 earthquake also stroke the city in 1962 (Aliaj et al., 2010; Jouanne et al., 2012, and Fig. 3-A). Between 2004 and 2017, 93 shallow earthquakes (above 15 km depth) occurred less than 15 km away from the Marinza village, among which 5 M_w 4+. In particular, a M_w 4.1 event occurred in December 2016 west of Zharrez, very near to the 1962 epicenter (Fig. 3-A). This event led the government to order a temporary break in the injection activities (Report CAO, 2018).

15 Two focal mechanisms are provided in the area by the CMT catalogue, for M_w4+ earthquakes that occurred at 6 and 10 km depth for the southern (2011) and northern (1997) events, respectively (Fig. 3-A). Both earthquakes exhibit clear strike-slip

motion that is consistent with the reactivation of faults affecting the Ionian limestone units. However, due to inadequate spatial coverage by seismic arrays, the precise depth of these events remains uncertain.

Keeping in mind that the seismic record in the zone may be incomplete due to the sparse seismic network, we calculate the cumulative moment evolution over the study area based on worldwide databases starting in 1990 (USGS and EMSC catalogues,

5 Fig. 3-B). Overall, in contrast with the period between 1990 to 2007, which is characterized by the occurrence of few moderate earthquakes, the cumulative released moment has been rising steadily since then, contemporaneously with the increase in oil production. Investigating on the causal link that may exist between the oil extraction activity and this increase in seismic moment release would require a fine monitoring of the background seismicity in this tectonically active region over a long period. Unfortunately, this information is currently lacking. Following a complaint filled by the population to an independent

10 office (the Compliance Advisor Ombudsman, CAO) after the 2013 seismic crisis (Fig. 3 and Report CAO, 2018), two broadband stations have been installed by researchers from University Polytechnics of Tirana in the central part of the oil field starting in September 2016, in order to record the intense seismic activity of the zone. However, because only two seismometers were installed, earthquake locations for small magnitude events are subject to large uncertainty and the observations have remained inconclusive up to now (Report CAO, 2018). Geodetic techniques represent another indirect method to monitor the effect of oil

15 field exploitation. We present below an InSAR analysis of surface ground motion in the Patos-Marinza field area to investigate the potential link between the field exploitation and the present-day surface deformation.

3 InSAR data and processing

We use data from the European Space Agency (ESA) Sentinel-1 Synthetic Aperture Radar (SAR) constellation, consisting of two satellites launched respectively in April 2014 (S1A) and April 2016 (S1B). Sentinel-1 operates in a burst mode (the

20 so-called TOPS mode, De Zan and Guarnieri, 2006), which allows for generating images ~ 250 km wide across-track, acquired in three contiguous sub-swaths. Each Sentinel-1 satellite operates on a sun-synchronous orbit with a cycle time of 12 days. The two satellites are phased at 180°, enabling a revisit time of 6 days for interferometry. Due to the acquisition plan designed by ESA, systematic acquisitions are carried out over Europe, including Albania, providing an optimal temporal coverage for our area of interest. We process independently SAR data acquired on two overlapping tracks acquired in descending (T153) and

25 ascending (T175) geometries, consisting respectively of 120 and 109 images over the 2014–2018 period (Figs. S1, S2).

Sentinel-1 data processing is carried out using the NSBAS software (Doin et al., 2011), which includes routines from the ROI_PAC software (Rosen et al., 2004). The originality of NSBAS is to enable the application of a series of correction prior to phase unwrapping, in order to minimize unwrapping errors, which remain the first limitation of the InSAR techniques in areas of low coherence. The specific Sentinel-1 processing technique used in NSBAS is described in Grandin (2015) and Grandin

30 et al. (2016). After selecting the common bursts in our image set, a master image is chosen on the basis of its central position in terms of spatial baseline and time of acquisition within the image stack (Figs. S1, S2). We use the 30 m SRTM digital elevation model (Farr and Kobrick, 2000) to compute the simulation in the master geometry. Then, all slave images are coregistered to
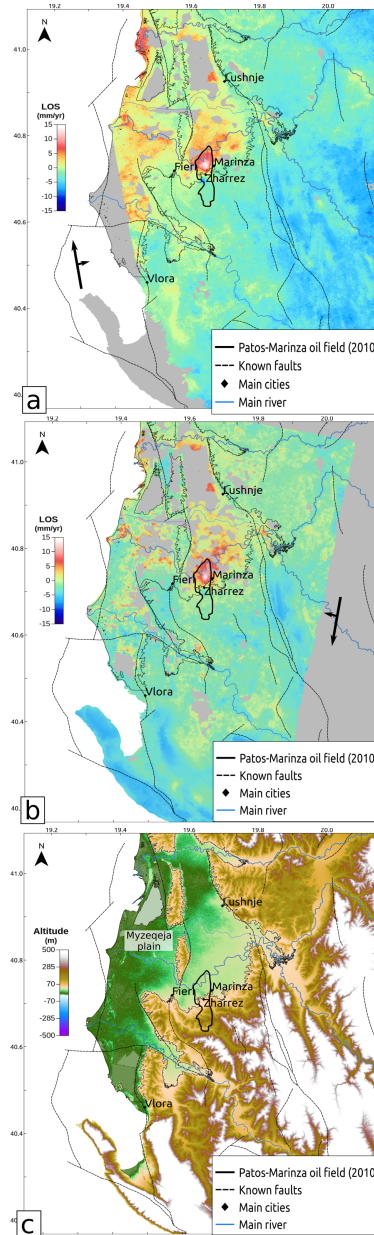
Figure 4. Large-scale view of the Line-Of-Sight (LOS) average velocity maps (positive values correspond to motion away from satellite, i.e. mostly subsidence), from time-series analysis of InSAR data along ascending (a) and descending (b) tracks, together with regional topography (c).

the master geometry using an affine transformation constrained by incoherent pixel correlation with the master image, and their simulated phase is computed using precise orbital information.

A network of small baseline interferograms (Berardino et al., 2002) is selected, minimizing spatial baselines, while retaining variety in temporal baselines and sufficient redundancy. A total of 512 interferograms are calculated on the descending track

5 (Fig S1), and 468 interferograms on the ascending track (Fig S2). Precise azimuthal coregistration is achieved by computing burst-overlap interferograms using the spectral diversity technique (Grandin et al., 2016). The residual azimuth offsets with respect to the master image are first evaluated using spectral diversity independently for each interferogram. They are then inverted within the interferogram network, in order to ensure consistency and mitigate potential ambiguity for poorly coherent interferograms. The resulting interferograms on adjacent sub-swaths are subsequently merged by solving for an integer number

10 of 2π shifts between the sub-swaths. We checked for the lack of phase jump across the sub-swaths borders and between the bursts.

Finally, atmospheric correction using the ECMWF's ERA-Interim atmospheric reanalysis is carried out using the method described in Jolivet et al. (2011) and Doin et al. (2009). Residual atmospheric delays correlated with topography are consistently inverted within the network using an empirical linear relation between phase and altitude. Similarly, large-scale phase ramps in

15 range, likely caused by residual large-scale atmospheric artifacts, are removed in a network-consistent manner. The resulting interferograms are filtered using a multiscale boxcar filter implemented in NSBAS. Phase unwrapping is also performed using a specific routine of NSBAS by propagating the unwrapping integration path across the interferogram, starting from a coherent reference pixel, and expanding progressively into areas of lower coherence (Grandin et al., 2012).

After unwrapping, all interferograms are registered to a reference area and a time-series inversion is carried out, in order to

20 solve for the temporal evolution of ground displacement between each acquisition date, and for the average velocity for each pixel independently (Figs. 4 to 6). Residual unwrapping errors are solved as part of the time-series inversion using an iterative technique (Cavalié et al., 2007, and references therein).

The median value of the interferometric network misclosure (root mean square in Fig. S3) is 0.5 rad and 1 rad for the descending and ascending tracks, respectively. We choose to mask pixels on velocity maps (Fig. 4) based on the number of

25 interferograms used to estimate the velocity. The minimum number of coherent interferograms required for each pixel is fixed to 370 for each track (75% the interferogram, Fig. 4).

4 Results

We extract the average linear Line-Of-Sight (LOS) velocity from the raw displacement time-series of both ascending and descending tracks (Fig. 4) by simultaneously estimating for each pixel the amplitude of annual and semi-annual sinusoidal signals

30 using the least-squares inversion strategy of Daout et al. (2017) (Fig. S4). The ascending track exhibits higher levels of annual variations than the descending one, in particular at the coast and at high altitudes. This may result from a significantly higher tropospheric variability at the acquisition time of the ascending track (6:33 PM local time, i.e. dusk), whereas acquisitions in

the descending track take place in more quiet atmospheric conditions (6:45 AM local time, i.e. dawn). However, in general, the level of annual and semi-annual variations is very low for both tracks over the Patos-Marinza oil field (Fig. S4).

The average LOS velocity maps shown in Figure 4 for both tracks exhibit very consistent deformation patterns and are highly correlated (r=0.97, Fig. S6). This similarity implies that the surface displacement is weakly dependent on the LOS vector and is

5 therefore mainly vertical. In the following, we will interpret the LOS velocities as nearly vertical motion, neglecting the small horizontal component. For further comparison purposes, we remove a uniform constant (3.24 mm/yr) from the descending LOS velocity map (as determined in Figure S6) to match it with the ascending one. We then calculate the covariogram for each velocity map, based on a stable zone covered by both tracks south of the Myzeqeja plain (Fig. S6). Both maps have a similar variance for zero distance but covariance is slightly higher at intermediate distances (10 to 20 km) for the descending map than

10 for the ascending one. This is consistent with the patchy deformation that can be observed at this kilometric scale only in the descending velocity map (Fig. 5).

The primary feature of these surface velocity maps is the subsidence of the whole Myzeqeja plain (Fig. 2, relative motion away from the satellite of ~2.5 mm/yr in average) with respect to the surrounding highlands that show no significant deformation (Figs. 4 and 5). However, subsidence is not uniform over the alluvial and deltaic basin and higher subsidence rates can be

15 locally observed (Fig. 5) (i) along the Semani River (5 to 10 mm/yr in LOS direction), (ii) west of Lushnje (~10 mm/yr), (iii) at the mouth of the Shkumbini River (~10 mm/yr) and (iv) concentrated in a 2.1 km by 2.1 km area in the northern part of the Patos-Marinza oil field with the highest rates (up to 20 mm/yr). We also identify a small uplifting area (~5 mm/yr in the LOS direction), roughly circular, immediately south of the maximum subsiding area and of the Zharrez village (Figs. 5 and 6).

Figure 6 shows the displacement time-series of these most subsiding and uplifting areas in the oil field with respect to a

20 stable zone: both trends are very linear on the 2014-2018 time-span, with no jump associated with the main events that affected the oil field during this period (gas leakage and M_w4+ earthquake), or oscillations that could be related to the seasonal or annual hydrological loading. The higher temporal resolution (return time of 6 days) available in the area since the end of 2016 will help tracking small and sudden deviations from the average trend in future studies. We limit our analysis below to that of the average velocity field.

25 ## 5 Discussion and modeling

5.1 Subsidence of the Myzeqeja plain

The striking dichotomy between the slowly subsiding Myzeqeja alluvial to deltaic plain (~2.5 mm/yr, Fig. 5) and the stable surrounding calcareous and molassic highlands argues in favour of a compaction phenomenon, widely observed in poorly consolidated alluvial and deltaic systems (e.g. Liu et al., 2004; Higgins, 2016, and references therein). Several natural processes

30 may be involved, among which compaction of clay layers due to the sediment net flux, isostatic adjustment, or seasonal and annual elastic or poro-elastic rebound due to external loading. Human activities may also amplify the natural subsidence of alluvial and deltaic zones in several ways: (i) pumping of groundwater or other buried fluids can accelerate the compaction process (e.g. Liu et al., 2004), (ii) changes in the hydrographic network can dramatically modify the streamflow paths, the
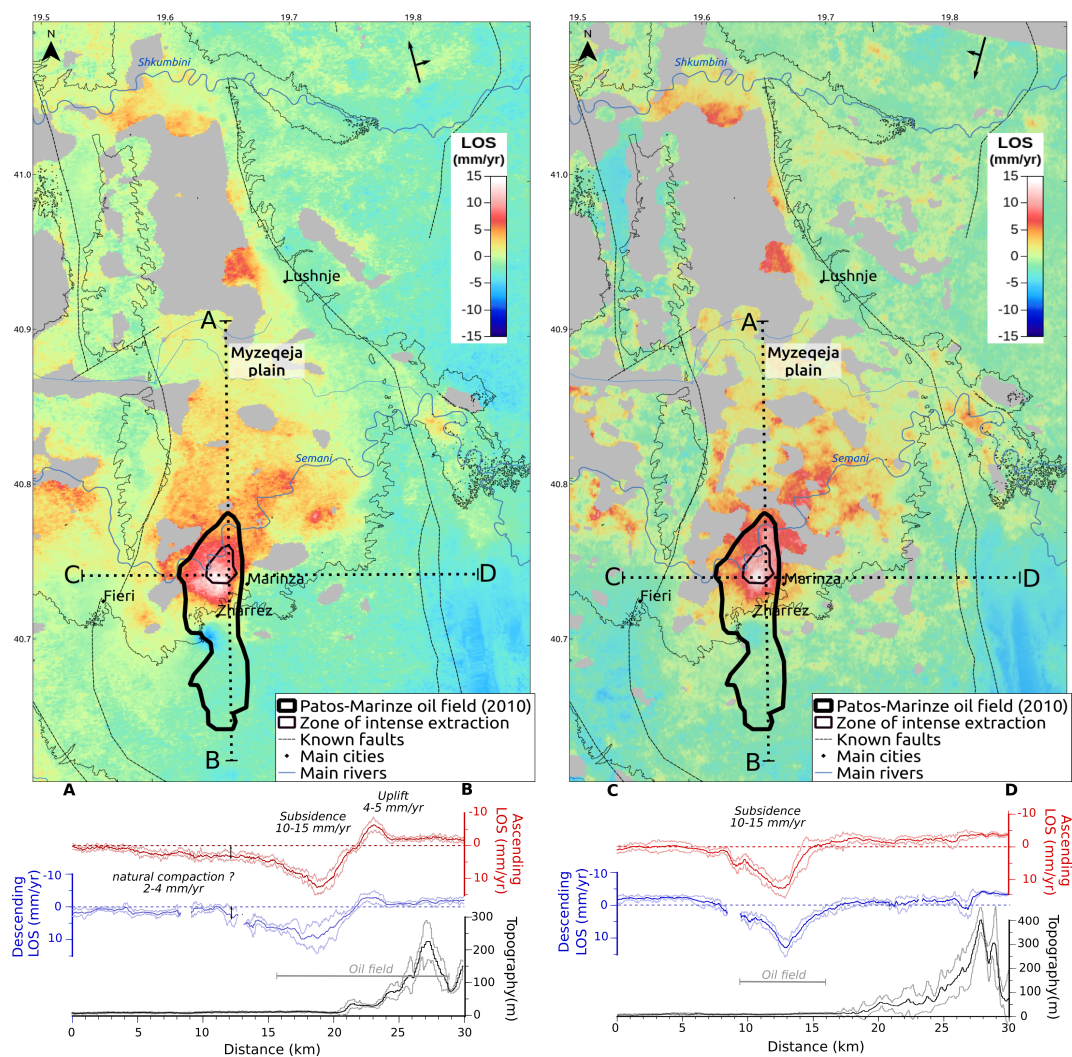
Figure 5. Top: Zoom on the LOS average velocity map for the ascending (left) and descending (right) tracks over the Patos-Marinza oil field. Color code and sign convention are the same as in Figure 4. Dotted lines indicate the location of the profiles at bottom. Bottom: north-south (left) and west-east (right) velocity profiles across the oil field's most intense deformation zone together with topography profiles (bottom). Average values over a 2 km width across the profile lines is plotted darker, while lighter lines limit the 2σ standard deviation envelop.
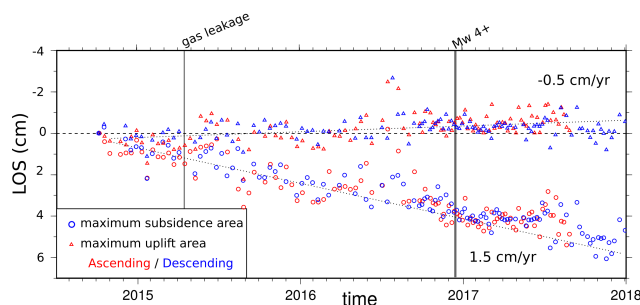
Figure 6. Displacement time-series for the most subsiding and uplifting areas (3x3 pixels) on both tracks (ascending is red, descending is blue) in the Patos-Marinza oil field, relative to a stable area. The average trend is indicated (dashed line), together with two particular events (grey vertical bars) related to the field exploitation and seismic activity.

water discharge and the net flux of sediments, and (iii) dense urbanization, as an external load, can favor compaction (e.g. Abidin et al., 2011).

All of these human subsidence-accelerating actions are at play in the Myzeqeja plain context. First, underground water coming from alluvial shallow aquifers is pumped for irrigation purposes and drinking water networks. Second, the marshy areas were recently reclaimed during the 1945 to 1980 period by building an extensive network of canals (Fig. 2-b, Shallari and Maughan, 2015). At last, the construction of dams upstream the Shkumbini and Semani rivers, of hill retention structures, and of breakwaters at the coast, have modified the sedimentary flux balance to the point that dramatic changes in the coastline have been observed between both rivers mouths (Ciavola and Simeoni, 1995; Ciavola, 1999; Bedini, 2007). Unravelling the different natural or anthropogenic sources of the plain subsidence is an arduous task and would require a fine knowledge of the water discharge, sediment budget, and mechanical behavior of the shallow sediment layers (Higgins, 2016). This problem is beyond the scope of this study. However, we suggest that the observed basin-wide subsidence is associated to a combination of natural and human-induced compaction. In particular, we interpret the high subsidence values observed along the Semani River and the Shkumbini River mouth as the consequence of the incessant deviations of their riverbeds and changes in the incoming sedimentary flux (Ciavola, 1999). A large part of the basin has been masked west of Lushnje given our confidence criteria after time-series analysis (see section 3), but some rapid subsidence is still observed around this area. Since this zone is slightly under sea level and has long remained marshy (Ciavola, 1999; Shallari and Maughan, 2015, and Fig. 2), we interpret this local high subsidence rate as natural compaction associated with recent land reclamation. However, a longer time-series would be required to further analyze the specific behavior of this basin.

5.2 Deformation in the Patos-Marinza field

The LOS deformation pattern observed over the Patos-Marinza oil field differs in many ways from the diffuse subsidence of the Myzeqeja plain described above (Fig. 5). Looking at this mainly vertical deformation along north-south and west-east LOS velocity profiles highlights again the very good consistency between both tracks. The spatial correlation between the fast

subsidence zone and the active part of the oil field, intensely operated using horizontal drilling or waterflooding recovery, also appears clearly (Fig. 3). The slight uplift observed further to the south is located at the southern boundary of zones where thermal and infill recovery methods have been used according to BCP, 2010. This uplift is roughly circular and is very similar to deformation patterns that would be associated to local inflation of a buried source (Mogi, 1958; Lisowski, 2007). The shape

5   of the area of fast subsidence appears also nearly radial on the west-east profile but is superimposed with the overall subsidence of the alluvial plain on the north-south profile (Fig. 5). The nearly axi-symmetric shape of the observed surface deformation pattern, together with the clear spatial correlation between high subsidence rates and the zone where intense oil extraction is conducted, thus argue in favor of a local subsidence induced by reservoir compaction as observed elsewhere (e.g. Chaussard et al., 2013; Liu et al., 2015; Grebby et al., 2019).

10 Surface deformation has been monitored over a wide range of oil and gas fields worldwide and several physical models have been proposed and confronted to real data (e.g. van Thienen-Visser and Fokker, 2017). In the simplest elastic case, analytical solutions developed for buried points or finite spherical sources (Mogi, 1958), tensile dislocations (Okada, 1985), and circular sill-like horizontal cracks (Fialko et al., 2001), can provide first-order models for surface deformation due to buried volumetric or pressure changes. Analytical formulations based on the poroelastic theory have also been proposed in the

15 case of a compacting cylindrical reservoir to calculate the associated stress and displacement field in the medium (Geertsma et al., 1973; Segall et al., 1994; Goebel et al., 2017). The surface deformation field predicted by all of these physical models can differ significantly in the horizontal and vertical components (Lisowski, 2007). However, discriminating between these different physical models requires both horizontal and vertical components of surface deformation or the reservoir geometry to be known, which is not the case in our case study. Indeed, we lack information on the reservoir characteristics, and InSAR

20 is mainly sensitive to vertical motion (Dieterich and Decker, 1975; Lisowski, 2007; Fialko et al., 2001). We therefore adopt a two-step approach to best model the velocity field observed in the eastern Myzeqeja plain (Fig. 5).

First, we use the poroelastic formalism developed for an axisymmetric compacting reservoir by Segall (1989) to conduct a 1D simple inversion of the west-east LOS velocity profiles for both tracks presented in Figure 5. We invert for the depth, pressure change, radius and width of the compacting reservoir able to produce such a deformation pattern using simple least-

25 square optimisation. We fix the compaction coefficient to 3.10^9Pa^{-1} based on Weatherill et al. (2005), the Poisson ratio to 0.25, and we impose the depth to be shallower than 4.5 km. Both ascending and descending velocities are well reproduced by a 1045 m-long and 632 m-wide reservoir located at a depth of ~1.6 km under the zone of maximum subsidence in which pressure change is around 29.7 kPa/yr (see fit to the data in Fig. 7). These parameters are consistent with the average depth and width of the Driza and Marinza series that are the most intensely exploited Miocene units in the Patos-Marinza oil field

30 (Fig. 2-d). The observed surface subsidence would therefore correspond to a decrease of reservoir volume ΔV of roughly 0.2 Mm^3/yr on the 2014-2018 time-span.

The parameters adjusted using the previous simple poroelastic inversion are then used to fit the 2D velocity field using a simpler elastic formalism. We thus discretize the alluvial plain into 2.1 km×2.1 km horizontal tensile dislocations located at 1.6 km depth based on the poroelastic modeling (Fig. 7). Because of the scarce informations available about the reservoir geometry, we chose to use horizontal dislocations. It is also to note that because the dislocation depth is of the same order of
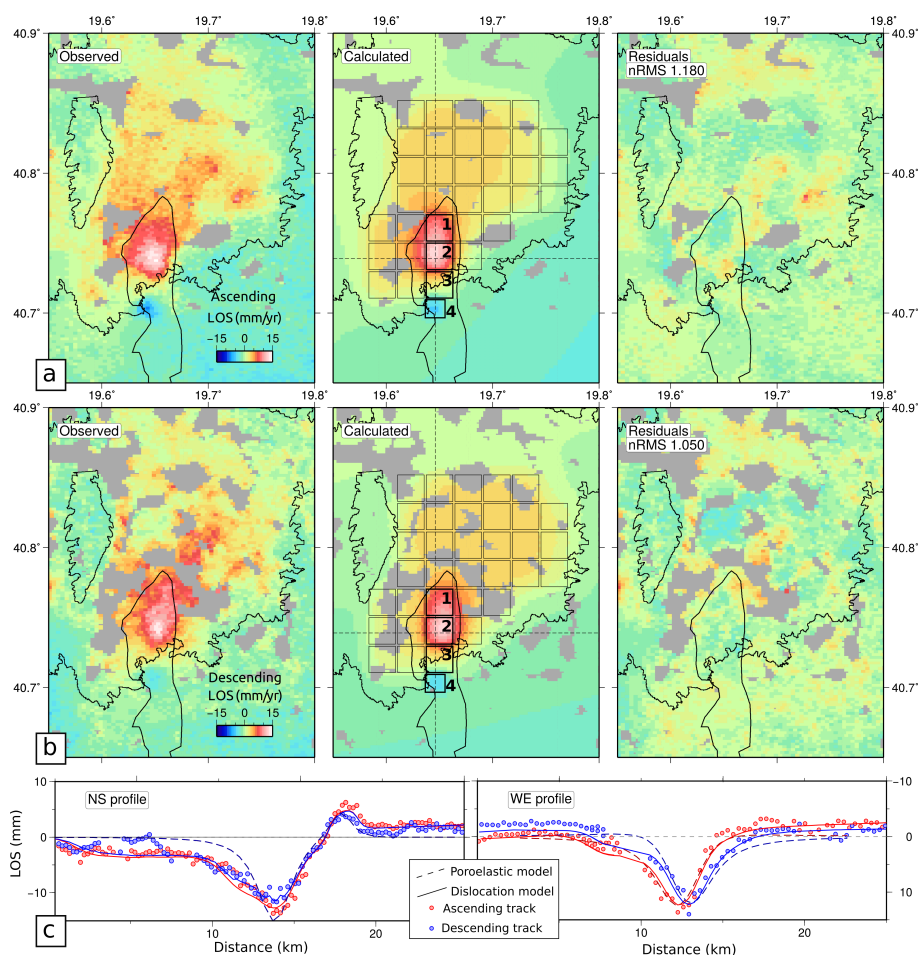
Figure 7. a,b- Calculated LOS velocity maps (left) are compared with predicted ones, produced by planar crack Okada-type dislocations in a homogeneous elastic half space (centre), for both the ascending (a) and descending (b) tracks. Residuals are plotted on the right panel. Grey dashed lines in central panel show location of profiles at bottom. Numbered dislocations contoured in bold are those inside the oil field (see text for details). c- north-south and west-east profiles with observed (dots) and predicted (lines) velocities using either the planar-cracks model presented above (plain line) or a 2D poroelastic axysymmetric reservoir (dashed line) (see text for details). Velocities on the ascending and descending tracks are shown in red and blue. Note that the 2D poroelastic model predicts LOS-independent velocity curves in the NS direction.

Dislocation	Depth (km)	Surface (km^2)	ΔV (Mm^3/yr)
1	1.6	4.41	**-0.079**
2	1.6	4.41	**-0.120**
3	1.6	4.41	**-0.016**
4	**0.56**	**2.25**	**+0.015**
5-36	1.6	4.41	**-0.025**

Table 1. Parameters used in the best-fit multiple tensile dislocations model presented in Fig. 7. Dislocations inside the most intensively exploited part of the oil field are numbered from 1 to 4. Parameters adjusted during the inversion are plotted in bold characters.

magnitude as its size, we are at the limit of validity of the elastic approximation (Lisowski, 2007). The dislocations located outside the oil field will mimic the natural compaction effect described in section 5.1 that homogeneously affects the plain: the amount of tensile slip on these dislocations is therefore forced to be homogeneous over the entire basin (see Table 1). On the contrary, the amount of opening/closing of the dislocations located inside the most intensively exploited part of the oil field

5 (numbered from 1 to 4) are independent parameters. Since the spatial wavelength of the uplifting signal is significantly smaller than the breadth of the subsiding area, we allow the depth of dislocation number 4 over the uplifting area to vary between 0 and 4.5 km. We use the Tdefnode code developed by McCaffrey (2009) to invert for the amplitude of tensile slip on each dislocation as well as the depth and size of dislocation 4. The code is also free to search for a constant and linear ramps in the EW and NS direction to adjust tightly the two inverted velocity maps taking into account the local LOS vectors. Finally, 14

10 free parameters are adjusted.

This multiple planar cracks model produces a non radial deformation pattern that fits very well both observed velocity maps with normalized Root Mean Square (nRMS) close to 1 (Fig. 7). We summarize in Table 1 the parameters used to build the final model presented in Figure 7. The dislocations located outside the oil field are all experiencing low amplitude compaction that results in an overall 2.5 mm/yr motion in the LOS. This approximate modeling approach is efficient to mimic the overall

15 basin subsidence but is not physically consistent with the actual compaction mechanism that is likely more distributed over the sedimentary pile. We therefore refrain from interpreting the volumetric changes associated to these dislocations and rather focus on the oil field deformation modeling.

Dislocations 1 to 3 are all experiencing compaction equivalent to a reservoir deflation of ~0.215 Mm^3/yr, i.e. of the same order of magnitude as the volumetric change found using a 1D poroelastic model. The only dislocation experiencing inflation

20 at a rate of 0.015 Mm^3/yr is dislocation number 4 located south of the Zharrez village where uplift is observed. It should be noted that this source is found to be very superficial and that the volume involved is more than one order of magnitude lower that the total volumetric deflation found in the intensely exploited region. We interpret the circular uplift located south of the Zharrez village as an indication of local fluid injection activity in the shallow part of the sedimentary pile that may be due to leakage of injection well or to wastewater injection associated to oil extraction. Indeed, localized uplift associated with these

25 activities has already been extensively described (e.g. Teatini et al., 2011).

Keeping in mind the limitations of the elastic assumptions to model surface deformation due to shallow reservoir deflation and the fact that our model settings do not take into account the complex geometry of the reservoirs, our findings show that the observed surface deformation pattern over the Patos-Marinza oil field is consistent with compaction of the Driza and Marinza reservoirs. The estimated deflation rate is relatively low (~0.215 Mm^3/yr) compared to the average volume of oil extracted on
5   an annual basis since 2014 (~1.16 Mm^3/yr, Fig. 3). This apparent discrepancy can be explained by several factors. First, the oil production is calculated by the operating company over the entire oil field. Therefore, this calculation takes into account oil that has been extracted everywhere in the field with different extraction techniques or in other reservoirs. Second, in the most intensely operated zone experiencing the highest subsidence rates, oil is extracted via horizontal drilling and waterflooding techniques (Fig. 3) that imply substantial injection of fluids indepth. The net volumetric change experienced by the reservoirs
10   is therefore lower than what would result from oil depletion alone (Pierce, 1970). Finally, to properly assess the net volumetric change of the reservoirs, one would need to build a 3D finite elements model of the media taking into account its physical properties, geometry, pressure history, etc., i.e. data we do not have access to at the moment.

6   Conclusions & implication for local seismic hazard

Albania is an earthquake-prone country where seismic hazard is high (Jouanne et al., 2012; Métois et al., 2015). Unfortunately,
15   local seismological arrays are still too sparse to provide accurate locations and focal mechanisms of the small magnitude earthquakes occurring in the vicinity of the Patos-Marinza oil field, a necessary pre-requisite to conclude on the induced nature of the recent increase in local seismicity (Fig. 3).

Nevertheless, the large subsidence rate observed by InSAR over the most intensely exploited zone of the oil field (up to ~15 mm/yr of vertical motion), which contrasts with the slow compacting rates in the Myzeqeja plain (~2.5 mm/yr of vertical
20   motion) and the slow uplifting rate to the south (up to 5 mm/yr), is a strong evidence that a significant man-induced compaction is occurring in the Patos-Marinza field. Such type of surface deformation is likely associated with stress changes in the neighboring geological formations, which have been correlated with low to intermediate magnitude seismicity in several well-instrumented oil fields (e.g. Segall et al., 1994; Ellsworth, 2013; Keranen et al., 2013, 2014; Hornbach et al., 2016). Induced seismicity is now routinely monitored by operating companies, together with the pressure evolution of the reservoirs and the
25   pressure history of each injection well, in order to avoid sharp stress changes that may favor seismic ruptures. Because they involve large amounts of injected fluids indepth for long periods, wastewater injection and EOR techniques are particularly prone to induce seismicity (Rubinstein and Mahani, 2015). We suggest that the amplitude and shape of the observed deformation in the Patos-Marinza oil field, together with the increase of the cumulative released seismic moment in the area that started in 2008 when the oil production resumed, are strong evidences that the intense oil extraction activity in the northern part of the
30   field may induce seismicity in the area.

The Ionian limestones that have been largely folded and thrusted are still tectonically active due to the ongoing compression in the external Albanides (Jouanne et al., 2012; Guzmán et al., 2014; Aliaj et al., 2000). The occurrence of the recent M$_w$ 5.7, Pawnee earthquake that broke a previously unknown basement fault under an intensely exploited hydrocarbon field in

Oklahoma (Grandin et al., 2017; Keranen et al., 2013), illustrates the fact that stress changes associated with subsurface human activities may affect a broad area and trigger significant earthquakes. Whether the stress changes associated with the oil extraction in the Patos-Marinza field may be sufficient to trigger earthquakes on underlying faults is therefore an open question that challenges the seismic-hazard assessment in the area. Denser and more precise seismic catalogues, together with longer

5 InSAR or other geodetic time-series to monitor the spatio-temporal evolution of the deformation, as well as detailed knowledge of the wells injection history and reservoir properties, will be essential to explore this issue further on.

Author contributions. M.B., C.L and R.G processed the radar images and produced the InSAR time-series. M.B. and M.M. modelled the data. L.B., R.K and E.D gave insights on the geological, seismological and industrial context. M.M coordinated the ALBA project, the redaction of the present paper. All authors participated in the interpretation and discussion of the results.

10 *Competing interests.* The authors declare no competing interests.

Acknowledgements. This research is part of the ALBA project funded by the CNES APR program. Significant support in the French-Albanese collaboration has been provided by the Université de Lyon Impulsion-Palse program granted to M.Métois. InSAR data were processed using the NSBAS chain, mainly developed at ISTerre and IPGP as part of a french community effort to provide tools for the Data & Services center for Solid Earth (ForM@Ter). The figures of this manuscript were done using the free and open source GMT library

15 (http://gmt.soest.hawaii.edu/) and the QGIS software (http://qgis.osgeo.org).

References

Abidin, H. Z., Andreas, H., Gumilar, I., Fukuda, Y., Pohan, Y. E., and Deguchi, T.: Land subsidence of Jakarta (Indonesia) and its relation with urban development, Natural Hazards, 59, 1753, 2011.

Aliaj, S., Sulstarova, E., Muço, B., and Kociu, S.: Seismotectonic map of Albania, scale 1: 500.000, Seismological Institute Tirana, p. 297, 2000.

Aliaj, S., Koçiu, S., Muço, B., and Sulstarova, E.: The seismicity, seismotectonics and seismic hazard assessment in Albania, Albanian Academy of Sciences, Tirana, 2010.

BCP, 2010: Albania: Bankers Petroleum - Developing Europe's largest onshore oilfield, https://www.energy-pedia.com/news/albania/bankers-petroleum---developing-europes-largest-onshore-oilfield, 2010.

BCP, 2015: Bankers corporate presentation 2015, https://www.bankerspetroleum.com/sites/default/files/presentations/pdfs/BNK-2015-July%20Corporate%20Presentation%20-%20V3%20-%20FINAL.pdf, July 2015.

Bedini, E.: Use of GIS and remote sensing to detect change along the coastline segment between Shkumbini and Semani rivers, central Albania, Δελτίον της Ελληνικής Γεωλογικής Εταιρίας, 40, 1916–1924, 2007.

Bennion, D., Mastmann, M., Moustakis, M., et al.: A case study of foamy oil recovery in the Patos-Marinza reservoir, Driza Sand, Albania, Journal of Canadian Petroleum Technology, 42, 2003.

Berardino, P., Fornaro, G., Lanari, R., and Sansosti, E.: A new algorithm for surface deformation monitoring based on small baseline differential SAR interferograms, IEEE transactions on geoscience and remote sensing, 40, 2375–2383, 2002.

CAO complaint, filed 13 March 2013: Albania / Bankers Petroleum-01 / Patos, http://www.cao-ombudsman.org/cases/case_detail.aspx?id=197, 2013.

Cavalié, O., Doin, M.-P., Lasserre, C., and Briole, P.: Ground motion measurement in the Lake Mead area, Nevada, by differential synthetic aperture radar interferometry time series analysis: Probing the lithosphere rheological structure, Journal of Geophysical Research: Solid Earth, 112, 2007.

Chaussard, E., Amelung, F., Abidin, H., and Hong, S.-H.: Sinking cities in Indonesia: ALOS PALSAR detects rapid subsidence due to groundwater and gas extraction, Remote Sensing of Environment, 128, 150–161, 2013.

Ciavola, P.: Relation between river dynamics and coastal changes in Albania: an assessment integrating satellite imagery with historical data, International Journal of Remote Sensing, 20, 561–584, 1999.

Ciavola, P. and Simeoni, U.: A review of the coastal geomorphology of Karavasta Lagoon (Albania): short term coastal change and implications for coastal conservation, 1995.

Contamination report, 2015: Patos-Marinza development project, Well 5761 ERP Contamination Assessment Report, https://www.bankerspetroleum.com/sites/default/files/Environmental%20Assessment%20Full%20Report%20-%20web.pdf, 2015.

Coplin, L. S. and Galloway, D.: Houston-Galveston, Texas, Land subsidence in the United States: US Geological Survey Circular, 1182, 35–48, 1999.

CSEM-EMSC: https://www.emsc-csem.org/.

Daout, S., Doin, M.-P., Peltzer, G., Socquet, A., and Lasserre, C.: Large-scale InSAR monitoring of permafrost freeze-thaw cycles on the Tibetan Plateau, Geophysical Research Letters, 44, 901–909, 2017.

De Zan, F. and Guarnieri, A. M.: TOPSAR: Terrain observation by progressive scans, IEEE Transactions on Geoscience and Remote Sensing, 44, 2352–2360, 2006.

Dieterich, J. H. and Decker, R. W.: Finite element modeling of surface deformation associated with volcanism, Journal of Geophysical Research, 80, 4094–4102, 1975.

Doin, M.-P., Lasserre, C., Peltzer, G., Cavalié, O., and Doubre, C.: Corrections of stratified tropospheric delays in SAR interferometry: Validation with global atmospheric models, Journal of Applied Geophysics, 69, 35–50, 2009.

5   Doin, M.-P., Guillaso, S., Jolivet, R., Lasserre, C., Lodge, F., Ducret, G., and Grandin, R.: Presentation of the small baseline NSBAS processing chain on a case example: the Etna deformation monitoring from 2003 to 2010 using Envisat data, in: Proceedings of the Fringe symposium, pp. 3434–3437, ES, 2011.

Doornhof, D., Kristiansen, T. G., Nagel, N. B., Pattillo, P. D., and Sayers, C.: Compaction and subsidence, Oilfield Review, 18, 50–68, 2006.

Ellsworth, W. L.: Injection-induced earthquakes, Science, 341, 1225 942, 2013.

10 Farr, T. G. and Kobrick, M.: Shuttle Radar Topography Mission produces a wealth of data, Eos, Transactions American Geophysical Union, 81, 583–585, 2000.

Fialko, Y., Khazan, Y., and Simons, M.: Deformation due to a pressurized horizontal circular crack in an elastic half-space, with applications to volcano geodesy, Geophysical Journal International, 146, 181–190, 2001.

Geertsma, J. et al.: Land subsidence above compacting oil and gas reservoirs, Journal of Petroleum Technology, 25, 734–744, 1973.

15 Goebel, T., Weingarten, M., Chen, X., Haffener, J., and Brodsky, E.: The 2016 Mw5.1 Fairview, Oklahoma earthquakes: Evidence for long-range poroelastic triggering at >40 km from fluid disposal wells, Earth and Planetary Science Letters, 472, 50–61, 2017.

Grandin, R.: Interferometric processing of SLC Sentinel-1 TOPS data, in: FRINGE?15: Advances in the Science and Applications of SAR Interferometry and Sentinel-1 InSAR Workshop, Frascati, Italy, 23-27 March 2015, 2015.

Grandin, R., Doin, M.-P., Bollinger, L., Pinel-Puysségur, B., Ducret, G., Jolivet, R., and Sapkota, S. N.: Long-term growth of the Himalaya
20 inferred from interseismic InSAR measurement, Geology, 40, 1059–1062, 2012.

Grandin, R., Klein, E., Métois, M., and Vigny, C.: Three-dimensional displacement field of the 2015 Mw8. 3 Illapel earthquake (Chile) from across-and along-track Sentinel-1 TOPS interferometry, Geophysical Research Letters, 43, 2552–2561, 2016.

Grandin, R., Vallée, M., and Lacassin, R.: Rupture process of the Mw 5.8 Pawnee, Oklahoma, earthquake from Sentinel-1 InSAR and seismological data, Seismological Research Letters, 88, 994–1004, 2017.

25 Grebby, S., Orynbassarova, E., Sowter, A., Gee, D., and Athab, A.: Delineating ground deformation over the Tengiz oil field, Kazakhstan, using the Intermittent SBAS (ISBAS) DInSAR algorithm, International Journal of Applied Earth Observation and Geoinformation, 81, 37–46, 2019.

Guzmán, O., Mugnier, J.-L., Vassallo, R., Koçi, R., and Jouanne, F.: Vertical slip rates of active faults of southern Albania inferred from river terraces, Annals of Geophysics, 56, 2014.

30 Hettema, M. H., Jaarsma, B., Schroot, B. M., and van Yperen, G. C.: An empirical relationship for the seismic activity rate of the Groningen gas field, Netherlands Journal of Geosciences, 96, s149–s161, 2017.

Higgins, S. A.: Advances in delta-subsidence research using satellite methods, Hydrogeology Journal, 24, 587–600, 2016.

Hornbach, M. J., Jones, M., Scales, M., DeShon, H. R., Magnani, M. B., Frohlich, C., Stump, B., Hayward, C., and Layton, M.: Ellenburger wastewater injection and seismicity in North Texas, Physics of the Earth and Planetary Interiors, 261, 54–68, 2016.

35 Jolivet, R., Grandin, R., Lasserre, C., Doin, M.-P., and Peltzer, G.: Systematic InSAR tropospheric phase delay corrections from global meteorological reanalysis data, Geophysical Research Letters, 38, 2011.

Jouanne, F., Mugnier, J., Koci, R., Bushati, S., Matev, K., Kuka, N., Shinko, I., Kociu, S., and Duni, L.: GPS constraints on current tectonics of Albania, Tectonophysics, 554, 50–62, 2012.

Keranen, K. M., Savage, H. M., Abers, G. A., and Cochran, E. S.: Potentially induced earthquakes in Oklahoma, USA: Links between wastewater injection and the 2011 Mw 5.7 earthquake sequence, Geology, 41, 699–702, 2013.

Keranen, K. M., Weingarten, M., Abers, G. A., Bekins, B. A., and Ge, S.: Sharp increase in central Oklahoma seismicity since 2008 induced by massive wastewater injection, Science, 345, 448–451, 2014.

5 Lisowski, M.: Analytical volcano deformation source models, in: Volcano deformation, pp. 279–304, Springer, 2007.

Liu, C.-H., Pan, Y.-W., Liao, J.-J., Huang, C.-T., and Ouyang, S.: Characterization of land subsidence in the Choshui River alluvial fan, Taiwan, Environmental Geology, 45, 1154–1166, 2004.

Liu, P., Li, Q., Li, Z., Hoey, T., Liu, Y., and Wang, C.: Land subsidence over oilfields in the Yellow River Delta, Remote Sensing, 7, 1540–1564, 2015.

10 McCaffrey, R.: Time-dependent inversion of three-component continuous GPS for steady and transient sources in northern Cascadia, Geophysical Research Letters, 36, 2009.

Meço, S., Aliaj, S., and Bowen, R.: Geology of Albania, vol. 28, Gebr. Borntraeger, 2000.

Métois, M., D'Agostino, N., Avallone, A., Chamot-Rooke, N., Rabaute, A., Duni, L., Kuka, N., Koci, R., and Georgiev, I.: Insights on continental collisional processes from GPS data: Dynamics of the peri-Adriatic belts, Journal of Geophysical Research: Solid Earth, 120,
15 8701–8719, 2015.

Mogi, K.: Relations between the eruptions of various volcanoes and the deformations of the ground surfaces around them, Earthq Res Inst, 36, 99–134, 1958.

Murray, K. E.: State-scale perspective on water use and production associated with oil and gas operations, Oklahoma, US, Environmental science & technology, 47, 4918–4925, 2013.

20 Nagel, N.: Compaction and subsidence issues within the petroleum industry: From Wilmington to Ekofisk and beyond, Physics and Chemistry of the Earth, Part A: Solid Earth and Geodesy, 26, 3–14, 2001.

Okada, Y.: Surface deformation due to shear and tensile faults in a half-space, Bulletin of the seismological society of America, 75, 1135–1154, 1985.

Ottemöller, L., Nielsen, H., Atakan, K., Braunmiller, J., and Havskov, J.: The 7 May 2001 induced seismic event in the Ekofisk oil field,
25 North Sea, Journal of Geophysical Research: Solid Earth, 110, 2005.

Pierce, R. L.: Reducing land subsidence in the wilmington oil field by use of saline waters, Water Resources Research, 6, 1505–1514, 1970.

Pratt, W. E. and Johnson, D. W.: Local subsidence of the Goose Creek oil field, The Journal of Geology, 34, 577–590, 1926.

Prifti, I. and Muska, K.: Hydrocarbon occurrences and petroleum geochemistry of Albanian oils, Italian Journal of Geosciences, 132, 228–235, 2013.

30 Report CAO, 2018: Dispute resolution conclusion report, Bankers Petroleum / Patos, Albania, http://www.cao-ombudsman.org/documents/BankersPetroleumDRConclusionReport_ENG.pdf, 2018.

Rosen, P. A., Hensley, S., Peltzer, G., and Simons, M.: Updated repeat orbit interferometry package released, Eos, Transactions American Geophysical Union, 85, 47–47, 2004.

Rubinstein, J. L. and Mahani, A. B.: Myths and facts on wastewater injection, hydraulic fracturing, enhanced oil recovery, and induced
35 seismicity, Seismological Research Letters, 86, 1060–1067, 2015.

satellite images from the Google Earth data base: Google satellite via Quick Map Service Plugin, https://satellites.pro/, last access: 2019-03-19.

Schoonbeek, J. et al.: Land subsidence as a result of natural gas extraction in the province of Groningen, in: SPE European Spring Meeting, Society of Petroleum Engineers, 1976.

Segall, P.: Earthquakes triggered by fluid extraction, Geology, 17, 942–946, 1989.

Segall, P., Grasso, J.-R., and Mossop, A.: Poroelastic stressing and induced seismicity near the Lacq gas field, southwestern France, Journal
5   of Geophysical Research: Solid Earth, 99, 15 423–15 438, 1994.

Sejdini, B., Constantinescu, P., and Piperi, T.: Petroleum exploration in Albania, in: Hydrocarbons of eastern central Europe, pp. 1–27, Springer, 1994.

Shallari, A. and Maughan, N.: Les zones humides littorales de la plaine albanaise. Reflet des évolutions socio-économiques en Albanie (1945-2015), Méditerranée. Revue géographique des pays méditerranéens/Journal of Mediterranean geography, pp. 165–187, 2015.

10   Shebalin, N., Leydecker, G., Mokrushina, N., Tatevossian, R., Erteleva, O., and Vassiliev, V. Y.: Earthquake catalogue for central and south-eastern Europe 342 BC–1990 AD, Final report to contract ETNU-CT93-0087, 1998.

Silo, V., Muska, K., and Silo, E.: Hydrocarbon evaluation aspects in Neogene clastic reservoirs, Vlora-Elbasan region, Albania, Italian Journal of geosciences, 132, 220–227, 2013.

Teatini, P., Gambolati, G., Ferronato, M., Settari, A., and Walters, D.: Surface uplift and time-dependent seismic hazard due to fluid injection
15   in eastern Texas, Journal of Geodynamics, 51, 1–16, 2011.

TPGINC: GIS database for physical Albania, http://gis.tpginc.net/albania, last access: 2019-03-19.

USGS: https://earthquake.usgs.gov/earthquakes/search/, last access : February 2019.

van Elk, J., Doornhof, D., Bommer, J. J., Bourne, S. J., Oates, S. J., Pinho, R., and Crowley, H.: Hazard and risk assessments for induced seismicity in Groningen, Netherlands Journal of Geosciences, 96, s259–s269, 2017.

20   van Thienen-Visser, K. and Fokker, P. A.: The future of subsidence modelling: compaction and subsidence due to gas depletion of the Groningen gas field in the Netherlands, Netherlands Journal of Geosciences, 96, s105–s116, 2017.

van Thienen-Visser, K., Pruiksma, J., and Breunese, J.: Compaction and subsidence of the Groningen gas field in the Netherlands, Proceedings of the International Association of Hydrological Sciences, 372, 367–373, 2015.

Velaj, T.: The structural style and hydrocarbon exploration of the subthrust in the Berati anticlinal belt, Albania, Journal of Petroleum
25   Exploration and Production Technology, 5, 123–145, 2015.

Verani, P. and Ineichen, G.: I Petroli dell'Albania, La rivista italiana del petrolio, 5, 1942.

Walsh, F. R. and Zoback, M. D.: Oklahoma's recent earthquakes and saltwater disposal, Science advances, 1, e1500 195, 2015.

Weatherill, B., Seto, A. C., Gupta, S. K., Çobo, L., et al.: Cold heavy oil production at Patos-Marinza, Albania, in: SPE International Thermal Operations and Heavy Oil Symposium, Society of Petroleum Engineers, 2005.

30   Xhomo, A., Kodra, A., Dimo, L., Xhafa, Z., Nazaj, S., Nakuçi, V., Yzeiraj, D., Lula, F., Sadushi, P., Shallo, M., et al.: Geological Map of Albania 1: 200 000 scale, Republika e Shqiperise: Ministria e Industrise dhe Energjitikes, Ministria e Arsimit dhe Shkences, Sherbimi Gjeologjik Shqiptar, Albpetroli, Universiteti Politeknik i Tiranes, Tirana, 2002.